Research Article Vol. 3, No. 6 / June 2016 / Optica 597

Efficient microwave to optical photon conversion: an electro-optical realization

Alfredo Rueda,[1,2,3,†] Florian Sedlmeir,[1,2,3,9,†] Michele C. Collodo,[1,2,4,5] Ulrich Vogl,[1,2] Birgit Stiller,[1,2,6] Gerhard Schunk,[1,2,3] Dmitry V. Strekalov,[1] Christoph Marquardt,[1,2] Johannes M. Fink,[4,7] Oskar Painter,[4] Gerd Leuchs,[1,2] and Harald G. L. Schwefel[8,*]

[1]Max Planck Institute for the Science of Light, Günther-Scharowsky-Straße 1/Building 24, 90158 Erlangen, Germany
[2]Institute for Optics, Information and Photonics, University Erlangen-Nürnberg, Staudtstr. 7/B2, 91058 Erlangen, Germany
[3]SAOT, School in Advanced Optical Technologies, Paul-Gordan-Str. 6, 91052 Erlangen, Germany
[4]Institute for Quantum Information and Matter and Thomas J. Watson, Sr., Laboratory of Applied Physics, California Institute of Technology, Pasadena, California 91125, USA
[5]Currently at: Department of Physics, ETH Zürich, CH-8093 Zürich, Switzerland
[6]Currently at: Centre for Ultrahigh Bandwidth Devices for Optical Systems (CUDOS), School of Physics, University of Sydney, New South Wales 2006, Australia
[7]Currently at: Institute of Science and Technology Austria, 3400 Klosterneuburg, Austria
[8]Department of Physics, University of Otago, Dunedin, New Zealand
[9]e-mail: Florian. Sedlmeir@mpl.mpg.de
*Corresponding author: Harald. Schwefel@otago.ac.nz

Received 17 February 2016; revised 5 May 2016; accepted 13 May 2016 (Doc. ID 259508); published 6 June 2016

Linking classical microwave electrical circuits to the optical telecommunication band is at the core of modern communication. Future quantum information networks will require coherent microwave-to-optical conversion to link electronic quantum processors and memories via low-loss optical telecommunication networks. Efficient conversion can be achieved with electro-optical modulators operating at the single microwave photon level. In the standard electro-optic modulation scheme, this is impossible because both up- and down-converted sidebands are necessarily present. Here, we demonstrate true single-sideband up- or down-conversion in a triply resonant whispering gallery mode resonator by explicitly addressing modes with asymmetric free spectral range. Compared to previous experiments, we show a 3 orders of magnitude improvement of the electro-optical conversion efficiency, reaching 0.1% photon number conversion for a 10 GHz microwave tone at 0.42 mW of optical pump power. The presented scheme is fully compatible with existing superconducting 3D circuit quantum electrodynamics technology and can be used for nonclassical state conversion and communication. Our conversion bandwidth is larger than 1 MHz and is not fundamentally limited.

OCIS codes: (190.4223) Nonlinear wave mixing; (230.2090) Electro-optical devices; (190.7220) Upconversion.

http://dx.doi.org/10.1364/OPTICA.3.000597

1. INTRODUCTION

Efficient conversion of signals between the microwave and the optical domain is a key feature required in classical and quantum communication networks. In classical communication technology, the information is processed electronically at microwave frequencies of several gigahertz. Due to high ohmic losses at such frequencies, the distribution of the computational output over long distances is usually performed at optical frequencies in glass fibers. The emerging quantum information technology has developed similar requirements with additional layers of complexity, concerned with preventing loss, decoherence, and dephasing. Superconducting qubits operating at gigahertz frequencies are promising candidates for scalable quantum processors [1–3], while the optical domain offers access to a large set of very well developed quantum optical tools, such as highly efficient single-photon detectors and long-lived quantum memories [4]. Optical communication channels allow for low transmission losses and are, in contrast to electronic ones, not thermally occupied at room temperature due to the high photon energies compared to $k_B T$.

To be useful for quantum information, a noiseless conversion channel with unity conversion probability has to be developed. For the required coupling between the vastly different wavelengths, different experimental platforms have been proposed, e.g., cold atoms [5,6], spin ensembles coupled to superconducting circuits [7,8], and trapped ions [9,10]. The highest conversion efficiency so far was reached via electro-optomechanical coupling, where a high-quality mechanical membrane [11,12] or a piezoelectric photonic crystal [13] provide the link between an electronic LC circuit and laser light. Nearly 10% photon number

conversion from 7 GHz microwaves into the optical domain was demonstrated in a cryogenic environment [12]. Efficient direct electro-optic modulation as demonstrated, for example, in integrated microstructures [14,15] has been discussed by Tsang [16,17] as an alternative approach. The resulting phase modulation creates sidebands symmetrically around the optical pump frequency, which can be described by sum frequency generation (SFG) and difference frequency generation (DFG). The process of SFG combines a microwave and an optical photon and creates a blueshifted photon (anti-Stokes). This process is fundamentally noiseless and hence does not lead to decoherence if the photon conversion efficiency approaches unity.

In the process of DFG, the microwave signal photon can stimulate an optical pump photon to decay into a red-shifted optical (Stokes) and an additional microwave photon. Such microwave parametric amplification adds a minimum amount of noise as the process can also occur spontaneously (spontaneous parametric down-conversion) without the presence of a microwave signal [18]. This spontaneous process can be used to generate entangled pairs of microwave and optical photons [17]. Above threshold, the spontaneous process can stimulate parametric oscillations generating coherent microwave radiation [19].

Significant improvements of electro-optic modulation were made in the recent years through the development of resonant modulators with high quality (Q) factors consisting of a lithium niobate whispering gallery mode (WGM) resonator coupled to a microwave resonator [20,21]. The best reported photon conversion efficiency so far was of the order of 0.0001% per mW optical pump power [21,22]. These implementations could not individually address either SFG or DFG, and therefore always include additional noise from the spontaneous process.

Electro-optic single-sideband conversion has been demonstrated in a lithium tantalate WGM resonator, where the optical pump and the optical signal were orthogonally polarized (type-I conversion) [23]. The highest efficiency in lithium niobate can be expected when signal and pump are polarized in parallel (type-0 conversion). It was discussed that single-sideband conversion in this case can be achieved by detuning the optical pump from its resonance [16] [see Fig. 1(a)], which increases the required pump power significantly.

We present a new take on the classical electro-optical modulation within a lithium niobate whispering gallery mode resonator, where single-sideband operation is made possible without detuning. This is achieved by exploiting asymmetries in the free spectral ranges between three neighboring optical resonances caused by avoided crossings, as schematically depicted in Fig. 1(b). Since the mode crossings are temperature dependent, they can be used to tune the microwave input frequency over several tens of MHz and to switch between SFG and DFG.

With this system, we reach a photon number conversion efficiency of 0.2% per milliwatt optical pump power, which is 3 orders of magnitude larger than in previous works [21,22]. The significant increase of the conversion efficiency is due to better optical and microwave Q factors and enhanced modal overlap. Embedding the WGM resonator within a closed three-dimensional microwave cavity allows us to strongly focus the microwave field into the optical mode volume. Furthermore, our system is fully compatible with superconducting circuit quantum electrodynamics [24,25], since the microwave cavity is designed to be placed in a cryostat and contains the whole converter.

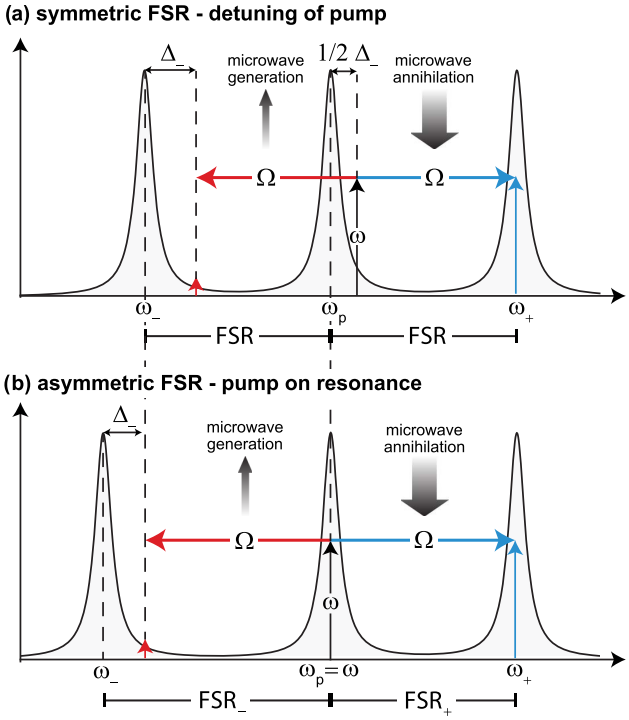

Fig. 1. Two schemes for suppressing the DFG signal in type-0 conversion are shown. (a) In the case of equally spaced modes, the optical pump has to be detuned to cause the red sideband to be off-resonant. (b) If the mode spacing is asymmetric, the pump can be kept fully resonant while maintaining the suppression of the undesired sideband.

Current state-of-the-art electro-optomechanical conversion schemes have a bandwidth of several kHz [11,12], and their bandwidth is fundamentally limited to the mechanical resonance frequency. The electro-optical scheme does not have this fundamental limitation. In the current implementation, we already reach a bandwidth of 1 MHz.

2. ALL-RESONANT ELECTRO-OPTICS

Our conversion scheme is based on the nonlinear interaction between resonantly enhanced microwave and optical fields within a high-quality WGM resonator. The optical resonator is made out of lithium niobate and is placed within a three-dimensional copper cavity. While the optical mode is guided at the rim of the WGM resonator by total internal reflection, the microwave field is confined by the metallic boundary of the copper cavity, which is designed to enforce good overlap of the optical and microwave modes within the lithium niobate. As lithium niobate is an electro-optic material, the microwave field modulates the refractive index and couples parametrically to the optical modes. Assuming weak microwave fields, only two sidebands (blue- and red-shifted) will be generated next to the optical pump frequency. The interaction Hamiltonian describing the system is

$$\hat{H}_{\mathrm{int}} = \underbrace{\hbar g_{-}(\hat{a}\hat{b}_{-}^{\dagger}\hat{c}^{\dagger} + \hat{a}^{\dagger}\hat{b}_{-}\hat{c})}_{\mathrm{DFG}} + \underbrace{\hbar g_{+}(\hat{a}\hat{b}_{+}^{\dagger}\hat{c} + \hat{a}^{\dagger}\hat{b}_{+}\hat{c}^{\dagger})}_{\mathrm{SFG}}, \quad (1)$$

where the operators $\hat{a}$, $\hat{b}_{+}$, $\hat{b}_{-}$ denote the optical pump and the up- and down-converted optical sidebands, respectively, and $\hat{c}$ denotes

the microwave mode. The nonlinear coupling rates $g_\pm$ are given by (compare e.g., [21])

$$g_\pm = \frac{n_p n_\pm}{n_\Omega} r \sqrt{\frac{\hbar \omega_p \omega_\pm \Omega_0}{8\epsilon_0 V_p V_\pm V_\Omega}} \times \int \mathrm{d}V \Psi_p \Psi_\Omega \Psi_\pm, \quad (2)$$

where n_p, $n_\pm$, and n_Ω are the refractive indices of the pump, sidebands, and the microwave tone and ω_p, $\omega_\pm$, and Ω_0 are the respective resonance frequencies. The normalization volumes V_p, $V_\pm$, and V_Ω are given by the integral $\int \mathrm{d}V \Psi\Psi^*$ over the respective spatial field distributions Ψ_p, $\Psi_\pm$, and Ψ_Ω. The nonlinear coupling is mediated by the electro-optic coefficient r. The integral in Eq. (2) is nonzero only if phase-matching is fulfilled. In the case of whispering gallery modes, this means that the azimuthal mode numbers m (number of wavelengths around the rim of the resonator) have to obey the relation $m_\pm = m_p \pm m_\Omega$. In our experiment, the optical pump P_p and the microwave signal P_Ω are both undepleted (i.e., the nonlinear conversion efficiency depends linearly on the pump and signal intensities). From Eq. (1) we find the output power of the sidebands $P_\pm$ and the photon number conversion efficiency $\eta_\pm$ to be

$$P_\pm = \underbrace{\frac{8g^2}{\hbar\Omega} \frac{\gamma^2 \gamma_\Omega}{|\Gamma_p|^2 |\Gamma_\pm|^2 |\Gamma_\Omega|^2}}_{\zeta_\pm} P_p P_\Omega \quad \text{and} \quad \eta_\pm = \frac{\Omega}{\omega_\pm} \zeta_\pm P_p, \quad (3)$$

where

$$\Gamma_p = -i(\omega - \omega_p) + \gamma + \gamma', \quad (4a)$$

$$\Gamma_\Omega = -i(\Omega - \Omega_0) + \gamma_\Omega + \gamma'_\Omega, \quad (4b)$$

$$\Gamma_\pm = -i(\omega \pm \Omega - \omega_\pm) + \gamma + \gamma'. \quad (4c)$$

The expressions in Eq. (4) describe the detuning of the optical pump ω, the microwave Ω, and the generated sidebands $\omega \pm \Omega$ from their respective resonance frequencies. Since the optical modes have the same polarization and are close in frequency, we can assume the same coupling and loss rates γ and γ' for all of them. For the nonlinear coupling rates, we assumed $g = g_- = g_+$ following the same argument. Coupling and loss rate for the microwave mode are denoted as γ_Ω and γ'_Ω.

In case of zero detunings for all modes, the common figure of merit, the electro-optic cooperativity [17], can be expressed in terms of the given metrics as

$$G_0 = \frac{|\alpha g|^2}{\Gamma_\pm \Gamma_\Omega} \approx \frac{\Gamma_\pm \Gamma_\Omega}{4\gamma_\pm \gamma_\Omega} \eta_\pm, \quad (5)$$

where $|\alpha|^2$ corresponds to the number of pump photons in the resonator. The approximation on the right-hand side is valid for the linear regime of small conversion efficiencies as assumed for Eq. (3). The cooperativity can therefore be directly calculated from the cavity parameters and the measured photon conversion rate.

If the optical modes are spectrally equidistant, the suppression of one of the sidebands can be achieved by detuning the pump from its resonance frequency as schematically depicted in Fig. 1(a). However, detuning decreases the coupling of the pump to the cavity and therefore increases the required pump power significantly (see below). We propose an alternative scheme depicted in Fig. 1(b): the spectral distance, or free spectral range (FSR), can be asymmetric for the up- and down-converted modes. This would allow detuning of, for example, the down-converted light by $\Delta_- = \omega - \Omega - \omega_-$ while the pump and the up-converted light remain fully resonant. We will show that such dispersion engineering is possible by exploiting avoided crossings. Both schemes in Fig. 1 lead to a power suppression factor S between the sidebands of

$$S = \frac{P_+}{P_-} = \frac{\Delta_-^2}{(\gamma + \gamma')^2} + 1. \quad (6)$$

As the suppression depends only on the detuning of the down-converted sideband from its resonance, the two schemes can be compared in terms of the required pump power using Eq. (3). One can show with the help of Eqs. (3) and (6) that the detuning scheme requires $(S-1)/4 + 1$ times more pump power to produce the same suppression S. For example, 30 dB suppression would require about 250 times more pump power.

3. EXPERIMENTAL REALIZATION

The challenge in this experiment is to bring two resonant systems having largely different frequencies to interact. The design has to provide a good spatial overlap between microwave and optical modes, while the involved modes have to fulfill phase-matching and energy conservation. This requires careful tailoring of the system based on numerical simulations. Our starting point was to realize a suitable geometry where the optical FSR is approximately equal to the frequency of the resonant microwave mode ($m_\Omega = 1$) to fulfill energy conservation (see Fig. 1).

For the experiment, we fabricated a lithium niobate WGM resonator with a radius of $R = 2.4$ mm and thickness $d = 0.4$ mm by single-point diamond turning and subsequent polishing [26]. The resonator has a z-cut configuration, where the optic axis is aligned parallel to the symmetry axis. The disk is placed in a 3D microwave copper cavity as depicted in Figs. 2(a)–2(c), where it is clamped by two metallic rings that are designed to maximize the field overlap between the microwave and optical modes. A silicon prism is placed within the cavity, touching the WGM resonator for optical coupling. To enable critical coupling, the coupling plane of the prism is coated with a thermally grown silicon oxide layer serving as a spacer. As an optical pump, we use a narrow-band tunable laser ($\lambda \approx 1550$ nm) which can either be swept over or locked to a resonance via the Pound–Drever–Hall technique. Two holes in the copper cavity allow the optical pump light to enter and the light reflected and emitted from the WGM resonator to leave the cavity. This light is collected and analyzed by a photodiode and an optical spectrum analyzer (OSA). The microwave signal is coupled via a coaxial pin coupler mounted close to the WGM resonator into the cavity and analyzed with a vector network analyzer (VNA) in reflection. A metallic tuning screw is used to perturb the microwave field for fine adjustment of its resonance frequency. The whole setup is thermally stabilized at room temperature with mK precision by a proportional–integral–derivative controller and a thermoelectric element attached on the outer side of the closed copper cavity.

All fields are primarily polarized along the optic axis of the WGM resonator (TE type modes) as we aim for type-0 conversion. This allows us to address the largest electro-optic tensor element of lithium niobate ($r_{33} \approx 31$ pm/V [27]).

Figure 2(d) shows the tuning over a typical optical mode detected in reflection. We find coupling efficiencies of about 60%. Although the modes are critically coupled ($\gamma = \gamma'$), 40% of the light is reflected from the cavity due to imperfect spatial mode

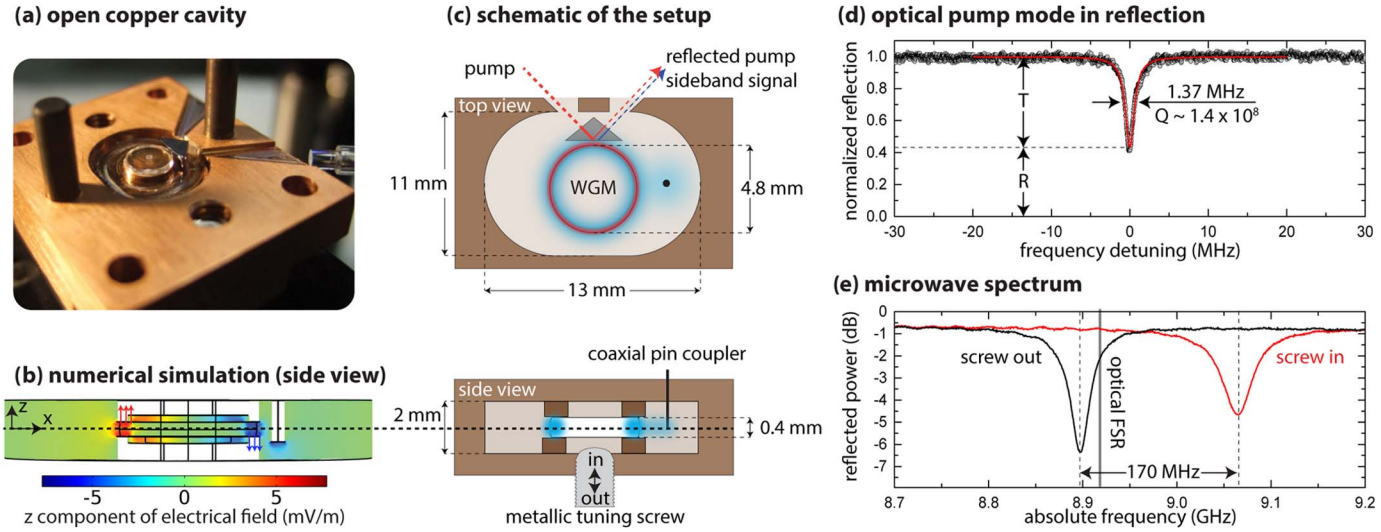

Fig. 2. (a) Photograph of the bottom part of the microwave cavity with silicon coupling prism and the WGM resonator. (b) Simulation of the microwave field distribution in the cavity. Only the z component (TE) of the field is shown. (c) Schematic of the cavity. An optical pump beam (red dashed) couples through a prism into the WGM, and part of the light is directly reflected. The sideband is given in blue. In the side view, the metallic tuning screw to perturb the microwave mode and the coaxial pin coupler are shown. The pin coupler is defined as the input port of the converter and the output port is the optical outcoupling spot inside of the prism (solid lines). (d) Reflection spectrum of the optical mode used for sum frequency conversion (compare Fig. 5). Also shown are the linewidth and the corresponding Q factors. (e) Microwave spectrum in reflection from the coaxial pin coupler. The $m_\Omega = \pm 1$ mode is shown for tuning screw position inside (red) and outside (black) the cavity.

matching. Typically the loaded Q is larger than 1×10^8, corresponding to linewidths less than 2 MHz. The optical free spectral ranges, which were measured with sideband spectroscopy [28], are around 8.95 GHz.

The phase and amplitude of the microwave signal back-reflected from the cavity was measured with the VNA. Figure 2(e) shows that the tuning screw allows us to change the microwave resonance frequency from $\Omega_0 = 2\pi \times 8.90$ GHz to $2\pi \times 9.07$ GHz. We find a loaded $Q = 246$ for the undisturbed mode, which decreases to $Q = 174$ for maximum perturbation by the tuning screw. Measurements of the phase response indicate that the microwave mode is undercoupled ($\gamma_\Omega < \gamma'_\Omega$), resulting in a nonideal coupling efficiency around 60%–75%, depending on the position of the tuning screw.

Note that the pin coupler in our current setup excites a propagating ($m_\Omega = 1$) and a counterpropagating ($m_\Omega = -1$) microwave mode and only the part propagating in the direction of the excited optical modes is converted. Considering these geometries and the analytic knowledge of the optical modes [29], we can rewrite Eq. (2) as $g_\pm = n_p^2 \omega_p r_{33} E_\Omega / 2$, where the single photon electric field E_Ω is determined from the simulated microwave field distribution in the region of the optical mode [compare Fig. 2(b)]. From this, we estimate the single-photon coupling rate for the $m = 1$ mode to be $g \approx 2\pi \times 28$ Hz.

A. Asymmetric FSR around Avoided Crossings

The key feature required for the single-sideband conversion in a WGM resonator with type-0 phase-matching without detuning the pump is an asymmetric spectral distance between the pump and the two signal modes (compare Fig. 1). In a mm-size resonator, adjacent free spectral ranges differ only by a couple of kHz due to the combined effect of material and geometric dispersion. Hence, both sidebands are generated in the case of zero pump detuning. However, in WGM resonators, different modes can couple to each other linearly if they are close to degeneracy [30,31]. Because of different thermal dispersion of different WGM families, such modes can be brought into resonance by changing the resonator temperature. This feature allows them to exchange energy and leads to avoided crossings. Such crossings appear as a mode splitting around the unperturbed resonance frequency, where the minimal spectral separation is proportional to the coupling rate between the two modes and can reach many linewidths. Essentially, the modes shift away from their unperturbed resonance position, leading to a change of the effective dispersion.

Such a crossing is shown in Fig. 3, where the frequency of a TE-polarized mode within a sweeping window of 100 MHz is plotted against a temperature change of the resonator. From the fit in Fig. 3 we extract a coupling rate of $\kappa = 2\pi \times 5.27$ MHz and the asymptotes, yielding the temperature dependence of the

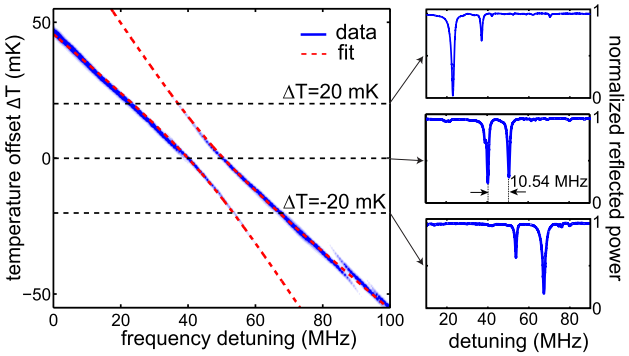

Fig. 3. On the left, the resonance position of a TE mode experiencing an avoided crossing with a TM mode is shown for different temperature settings. On the right, the WGM spectrum around the avoided crossing is plotted for different temperatures.

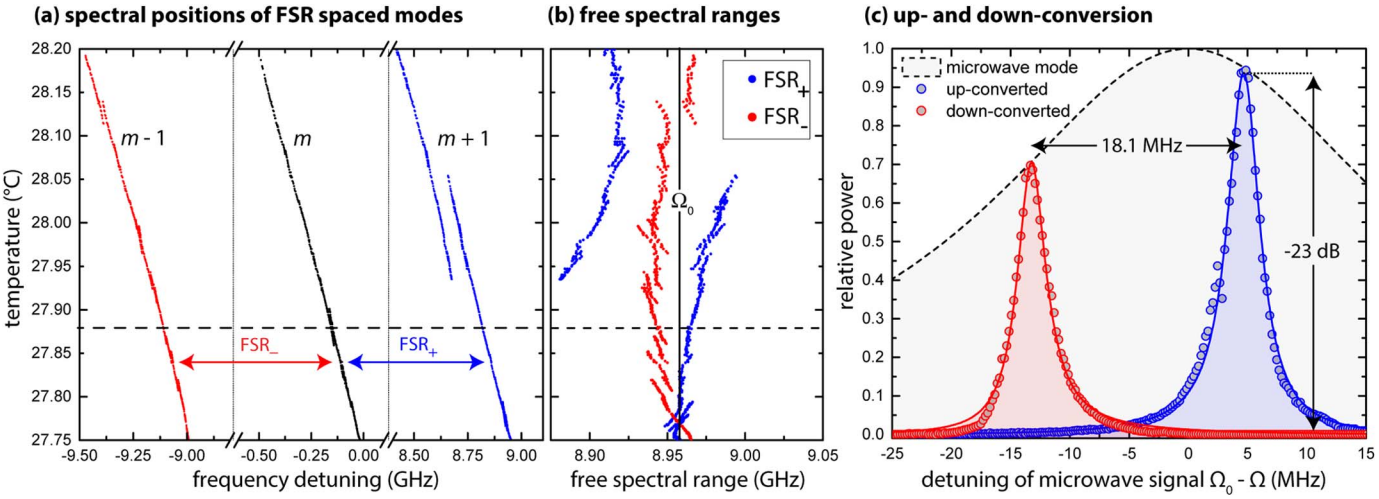

Fig. 4. (a) Resonance frequencies of three TE modes that are separated by one azimuthal mode number m corresponding to the free spectral range $\mathrm{FSR}_{\pm} \approx 9$ GHz. Each mode experiences avoided crossings of different strength for some temperatures. (b) Frequency difference of the $m+1$ and $m-1$ mode from the m mode. One can see that FSR_{+} and FSR_{-} are functions of the temperature and differ by up to 50 MHz. This allows selective up- and down-conversion as depicted in (c): The temperature was set to 27.88°C, indicated by the dashed line in (a) and (b), where $\mathrm{FSR}_{+} - \mathrm{FSR}_{-} = 18.1$ MHz. The optical pump is locked to the m mode. A microwave signal sweeping over the microwave resonance is indicated by the gray Lorentzian, while the generated sidebands are measured with an optical spectrum analyzer (see Fig. 5). The shown sidebands are separated by 18.1 MHz and the suppression of the down-conversion at the maximum of the up-conversion is about 23 dB.

two interacting modes. The ratio of their slopes is approximately 1.8, which corresponds to the ratio between the temperature sensitivities of TE and TM polarized modes in a lithium niobate WGM resonator of that size [32]. Such polarization coupling has been previously observed in ring resonators [33] and in larger magnesium fluoride resonators [34].

To demonstrate the effect of the splitting on the spectral distance between two adjacent modes of the same family, we show a spectrum of the $m-1$, m and $m+1$ modes in Fig. 4(a). The corresponding spectral distances $\mathrm{FSR}_{+} = \nu_{m+1} - \nu_m$ and $\mathrm{FSR}_{-} = \nu_m - \nu_{m-1}$ are presented in Fig. 4(b). The free spectral ranges are strongly temperature-dependent close to the avoided crossings, and the difference $|\Delta_{+} - \Delta_{-}|$ can be several tens of MHz, exceeding the linewidth of the modes significantly. We will use this temperature-dependent asymmetry of the FSR to switch between sum and difference frequency generation in the following sections.

B. Single-Sideband Conversion

For conversion of a microwave signal to a single optical sideband, we use the mode triplet shown in Figs. 4(a) and 4(b). The optical pump laser was locked to the central mode denoted with m (black curve), while the temperature of the cavity was stabilized around 27.88°C. The free spectral ranges at that working point are marked by the dashed line in Fig. 4(b). The microwave cavity resonance was set to $\Omega_0 = 2\pi \times 8.960$ GHz and the microwave signal sent to the cavity was swept from 8.925 to 8.975 GHz in steps of 200 kHz. For each step, the optical signal was measured with an optical spectrum analyzer (YOKOGAWA AQ6370C) (see inset in Fig. 5). The obtained magnitude of the generated sidebands is shown in Fig. 4(c) as a function of the microwave detuning from its resonance, which is indicated by the black dashed line.

The up- and down-converted signals can be addressed separately as they appear at different microwave frequencies due to the different FSRs of the respective modes. The Lorentzian given by Eq. (3) agrees well with the measured data. The asymmetry of the peaks and their intensity difference can be attributed to the detuning from the microwave resonance position. The central frequencies of the peaks are separated by 18.1 MHz, which corresponds to the difference between FSR_{+} and FSR_{-}. The extinction ratio for the suppressed sideband is determined by the FSR asymmetry and the linewidth of the microwave and optical modes. From the fit, we find a suppression of the down-converted signal at maximum up-conversion of 23 dB. This suppression could be further increased by a stronger mode splitting and narrower bandwidths of both the microwave and optical modes.

4. CONVERSION EFFICIENCY

The photon number conversion efficiency can be found by measuring the microwave power at the input and the optical signal power at the output of the converter. From Eq. (3), we find

$$\eta_{+} = \frac{\Omega}{\omega_{+}} \frac{P_{+}}{P_{\Omega}}. \tag{7}$$

As input power of the microwave, we take the power arriving at the coaxial pin coupler. Cable losses were calibrated out by measuring them separately prior to the experiment. As optical signal power, we consider the power leaving the WGM resonator inside the silicon prism [see Fig. 2(c)]. For this, we measured the reflection losses on the prism surface. This is justified for estimating the performance of the system because the prism can be coated to prevent reflection loss. The power of the sideband is obtained by measuring its relative strength compared with the reflected pump power on the optical spectrum analyzer. This allows us to calculate the sideband power leaving the resonator from the coupling efficiency of the pump and the absolute pump power sent to the resonator.

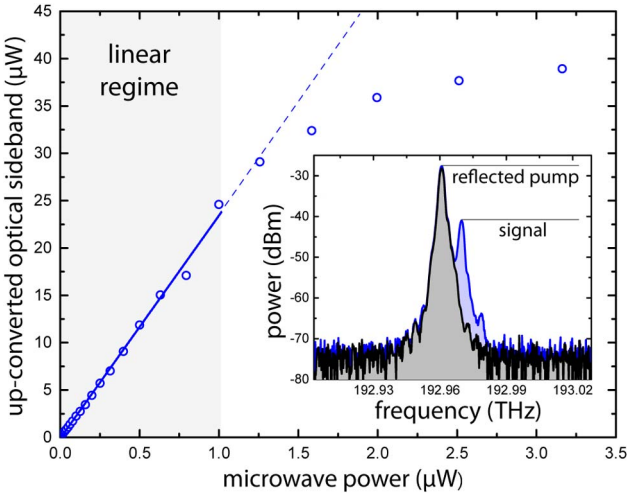

Fig. 5. Power of the up-converted sideband as a function of the microwave power sent to the cavity. With increasing microwave power, the optical pump mode depletes and the conversion efficiency decreases. A linear fit in the undepleted regime (gray) yields a slope of $P_+/P_\Omega = 23.68 \pm 0.46$, corresponding to a photon number conversion efficiency of $\eta_+ = (1.09 \pm 0.02) \times 10^{-3}$. The inset shows an OSA spectrum (resolution 2.5 GHz) of the reflected pump power and the generated up-converted sideband.

For demonstration of the absolute conversion efficiency, we choose the optical mode depicted in Fig. 2(d) and pump it on resonance. The working temperature is set such that the avoided crossing occurs on the red detuned side of the mode. This ensures that we can obtain a single sum-frequency-generated sideband which is not disturbed by the linear mode coupling causing the avoided crossing. We measure $\mathrm{FSR}_+ = 8.941$ GHz and adjust the microwave resonance frequency Ω_0 to that value with the tuning screw. In this configuration, we find $\gamma_\Omega = 2\pi \times 3.6$ MHz and $\gamma'_\Omega = 2\pi \times 16.2$ MHz for the undercoupled microwave mode and $\gamma = \gamma' = 2\pi \times 346$ kHz for the critically coupled optical mode. The laser is locked to the resonator, and 1 mW optical power is sent into the cavity. Considering the imperfect coupling and the resulting reflection from the prism [see Fig. 2(d)], 0.42 mW are actually coupled into the WGM resonator. The microwave signal frequency is set on resonance and the power is increased from −54 dBm to −22 dBm in steps of 1 dBm.

The results are presented in Fig. 5. The inset shows a typical OSA spectrum, where the single up-converted optical sideband is highlighted in blue. The plot shows the optical signal power leaving the resonator as a function of the input microwave signal power. In the undepleted pump regime, the optical signal scales linearly with the input microwave power according to Eq. (3). At approximately 1 μW microwave power, the pump starts to deplete and the up-converted signal saturates. From fitting the linear regime, we find a power conversion efficiency of $P_+/P_\Omega = 23.68 \pm 0.46$, which transforms into an absolute photon number conversion efficiency of $\eta_+ = (1.09 \pm 0.02) \times 10^{-3}$ using Eq. (7). Inserting the cavity parameters into Eq. (3), we find the single-photon coupling rate to be $g_{\mathrm{eff}} = 2\pi \times (7.43 \pm 0.02)$ Hz. In order to compare this value with the theoretically derived one, we have to multiply it by $\sqrt{2}$ since the theory does not take into account that we experimentally excite propagating and counterpropagating modes at the same time.

This effective coupling rate is about three times smaller than the expected one from numerical simulations, corresponding to almost ten times decreased conversion efficiency. This is likely caused by air gaps between the WGM resonator and the metallic rings clamping the resonator. Due to the high dielectric constant of lithium niobate in the microwave regime, even very small air gaps lead to a significant field drop in air. Our simulations show that an air gap of 20 μm caused by imperfect machining of the cavity and polishing of the upper and lower side of the WGM resonator lowers g already by a factor of 2.

5. DISCUSSION AND CONCLUSION

The three main findings of this paper are set forth in this section. The first is a 3 order of magnitude improvement of resonant electro-optic conversion of microwave photons into the optical regime compared to the so far best reported values [21,35]. The second is a highly efficient suppression of either the up- or down-converted sideband by engineering the dispersion of the resonator. The third is a MHz bandwidth for the conversion. All three findings are important steps towards coherent and bidirectional microwave photon conversion based on direct electro-optic modulation. For quantum operations, the conversion efficiency will have to be pushed toward unity, which is possible with some engineering improvements.

For high nonlinear coupling rates, the microwave mode starts to deplete in the case of SFG and the photon number conversion becomes [17]

$$\eta_+ = \frac{4\gamma\gamma_\Omega}{(\gamma+\gamma')(\gamma_\Omega+\gamma'_\Omega)} \frac{G_0}{(1+G_0)^2}. \tag{8}$$

It becomes apparent that $G_0 = 1$, $\gamma \gg \gamma'$, and $\gamma_\Omega \gg \gamma'_\Omega$ are required to approach unity photon number conversion. For our current system, which is critically coupled in the optical regime and undercoupled in the microwave regime, we find that $G_0 \approx 4 \times 10^{-3}$. Therefore, the cooperativity has to be enhanced by more than 3 orders of magnitude.

The pump power can be increased only slightly since photo- and thermo-refractive effects in lithium niobate cause the system to become unstable. While the optical Q factors are already close to the material limitation [36], it was shown recently that the intrinsic microwave absorption in lithium niobate at millikelvin temperatures allows for $Q_\Omega \approx 10^5$ [37]. This alone would increase our G_0 by 3 orders of magnitude in the current coupling regime. Furthermore, our simulations show that g scales inversely with the resonator thickness. Assuming a realistic resonator thickness of 50 μm, together with the closing of any air gaps deteriorating g, can improve the cooperativity additionally by 2 to 3 orders of magnitude. Recently, theoretical studies showed additional ways to increase g [38,39]. Putting these optimizations together, $G_0 \approx 1$ within an overcoupled regime can be achieved in a realistic scenario, ready to realize quantum state transfer [40]. Although optical cooling of the microwave mode will be possible to a certain extent, for quantum operation, the converter has to be operated in a cryostat to avoid up-conversion of thermal microwave photons. This is required anyway since it will increase the microwave Q factor due to superconducting boundaries and decrease of the dielectric loss in lithium niobate. Of course, this comes with additional challenges. Temperature tuning, for example, would have to be replaced by voltage tuning or pressure

tuning, and different thermal expansion of LN and the metal cavity have to be considered.

Electro-optomechanical schemes work in the resolved sideband regime where two pump tones, an optical and a microwave one, are detuned from their respective resonance frequencies by the mechanical resonance frequency. The consequence is that the bandwidth of the process is ultimately limited to the resonance frequency of the mechanical resonator, which is typically below 1 MHz. In practice, only tens of kilohertz have so far been achieved in efficient conversion experiments [12]. Coupling such systems to on-demand single-microwave photon sources [41] is challenging, as the temporal signature of these photons is in the order of megahertz [42]. Furthermore, the achievable suppression of the red-detuned sideband is limited as the pump detuning is also determined by the mechanical resonance frequency. Depending on the system parameters, this can lead to contamination of the converted signal with spontaneous emission.

Our system does not have these restrictions, as the mediator between the two regimes is the nonresonant, nonlinear polarizability of lithium niobate. Hence, the bandwidth of the electro-optic scheme is solely determined by intrinsic losses and the nonlinear as well as external coupling rates. Furthermore, the described dispersion management of the optical modes allows us to choose the degree of suppression freely, without detuning the optical pump.

These advantages justify the further investigation and optimization of the electro-optical approach, even though the electro-optomechanical approach presently has the efficiency advantage. As we have discussed, the single-photon regime is within reach provided an optimized system. This would not only allow for the interfacing of microwave qubits with the optical domain, but also electro-optic cooling of the microwave mode. With even lesser requirements, the generation of entangled pairs of microwave and optical photons utilizing parametric down-conversion is possible, which has recently been shown in the optical domain in a WGM-based system [43].

Funding. Alexander von Humboldt Foundation; Studienstiftung des Deutschen Volkes.

Acknowledgment. We would like to acknowledge our stimulating discussions with Konrad Lehnert and Alessandro Pitanti.

†These authors contributed equally to this work.

REFERENCES

1. R. J. Schoelkopf and S. M. Girvin, "Wiring up quantum systems," Nature **451**, 664–669 (2008).
2. M. H. Devoret and R. J. Schoelkopf, "Superconducting circuits for quantum information: an outlook," Science **339**, 1169–1174 (2013).
3. D. Ristè, S. Poletto, M.-Z. Huang, A. Bruno, V. Vesterinen, O.-P. Saira, and L. DiCarlo, "Detecting bit-flip errors in a logical qubit using stabilizer measurements," Nat. Commun. **6**, 6983 (2015).
4. A. I. Lvovsky, B. C. Sanders, and W. Tittel, "Optical quantum memory," Nat. Photonics **3**, 706–714 (2009).
5. M. Hafezi, Z. Kim, S. L. Rolston, L. A. Orozco, B. L. Lev, and J. M. Taylor, "Atomic interface between microwave and optical photons," Phys. Rev. A **85**, 020302 (2012).
6. J. Verdú, H. Zoubi, C. Koller, J. Majer, H. Ritsch, and J. Schmiedmayer, "Strong magnetic coupling of an ultracold gas to a superconducting waveguide cavity," Phys. Rev. Lett. **103**, 043603 (2009).
7. A. Imamoğlu, "Cavity QED based on collective magnetic dipole coupling: spin ensembles as hybrid two-level systems," Phys. Rev. Lett. **102**, 083602 (2009).
8. D. Marcos, M. Wubs, J. M. Taylor, R. Aguado, M. D. Lukin, and A. S. Sørensen, "Coupling nitrogen-vacancy centers in diamond to superconducting flux qubits," Phys. Rev. Lett. **105**, 210501 (2010).
9. L. A. Williamson, Y.-H. Chen, and J. J. Longdell, "Magneto-optic modulator with unit quantum efficiency," Phys. Rev. Lett. **113**, 203601 (2014).
10. X. Fernandez-Gonzalvo, Y.-H. Chen, C. Yin, S. Rogge, and J. J. Longdell, "Coherent frequency up-conversion of microwaves to the optical telecommunications band in an Er:YSO crystal," Phys. Rev. A **92**, 062313 (2015).
11. T. Bagci, A. Simonsen, S. Schmid, L. G. Villanueva, E. Zeuthen, J. Appel, J. M. Taylor, A. Sørensen, K. Usami, A. Schliesser, and E. S. Polzik, "Optical detection of radio waves through a nanomechanical transducer," Nature **507**, 81–85 (2014).
12. R. W. Andrews, R. W. Peterson, T. P. Purdy, K. Cicak, R. W. Simmonds, C. A. Regal, and K. W. Lehnert, "Bidirectional and efficient conversion between microwave and optical light," Nat. Phys. **10**, 321–326 (2014).
13. J. Bochmann, A. Vainsencher, D. D. Awschalom, and A. N. Cleland, "Nanomechanical coupling between microwave and optical photons," Nat. Phys. **9**, 712–716 (2013).
14. C. Xiong, W. H. P. Pernice, and H. X. Tang, "Low-loss, silicon integrated, aluminum nitride photonic circuits and their use for electro-optic signal processing," Nano Lett. **12**, 3562–3568 (2012).
15. L. Chen, Q. Xu, M. G. Wood, and R. M. Reano, "Hybrid silicon and lithium niobate electro-optical ring modulator," Optica **1**, 112–118 (2014).
16. M. Tsang, "Cavity quantum electro-optics," Phys. Rev. A **81**, 063837 (2010).
17. M. Tsang, "Cavity quantum electro-optics. II. Input-output relations between traveling optical and microwave fields," Phys. Rev. A **84**, 043845 (2011).
18. C. M. Caves, "Quantum limits on noise in linear amplifiers," Phys. Rev. D **26**, 1817–1839 (1982).
19. A. A. Savchenkov, A. B. Matsko, M. Mohageg, D. V. Strekalov, and L. Maleki, "Parametric oscillations in a whispering gallery resonator," Opt. Lett. **32**, 157–159 (2007).
20. D. Cohen, M. Hossein-Zadeh, and A. Levi, "Microphotonic modulator for microwave receiver," Electron. Lett. **37**, 300–301 (2001).
21. V. S. Ilchenko, A. A. Savchenkov, A. B. Matsko, and L. Maleki, "Whispering-gallery-mode electro-optic modulator and photonic microwave receiver," J. Opt. Soc. Am. B **20**, 333–342 (2003).
22. D. V. Strekalov, A. A. Savchenkov, A. B. Matsko, and N. Yu, "Efficient upconversion of subterahertz radiation in a high-Q whispering gallery resonator," Opt. Lett. **34**, 713–715 (2009).
23. A. A. Savchenkov, W. Liang, A. B. Matsko, V. S. Ilchenko, D. Seidel, and L. Maleki, "Tunable optical single-sideband modulator with complete sideband suppression," Opt. Lett. **34**, 1300–1302 (2009).
24. C. Rigetti, J. M. Gambetta, S. Poletto, B. L. T. Plourde, J. M. Chow, A. D. Córcoles, J. A. Smolin, S. T. Merkel, J. R. Rozen, G. A. Keefe, M. B. Rothwell, M. B. Ketchen, and M. Steffen, "Superconducting qubit in a waveguide cavity with a coherence time approaching 0.1 ms," Phys. Rev. B **86**, 100506 (2012).
25. H. Paik, D. I. Schuster, L. S. Bishop, G. Kirchmair, G. Catelani, A. P. Sears, B. R. Johnson, M. J. Reagor, L. Frunzio, L. I. Glazman, S. M. Girvin, M. H. Devoret, and R. J. Schoelkopf, "Observation of high coherence in Josephson junction qubits measured in a three-dimensional circuit QED architecture," Phys. Rev. Lett. **107**, 240501 (2011).
26. I. S. Grudinin, A. B. Matsko, A. A. Savchenkov, D. Strekalov, V. S. Ilchenko, and L. Maleki, "Ultra high Q crystalline microcavities," Opt. Commun. **265**, 33–38 (2006).
27. K. Wong, Properties of Lithium Niobate, EMIS Datareviews Series (INSPEC/Institution of Electrical Engineers, 2002).
28. J. Li, H. Lee, K. Y. Yang, and K. J. Vahala, "Sideband spectroscopy and dispersion measurement in microcavities," Opt. Express **20**, 26337–26344 (2012).
29. I. Breunig, B. Sturman, F. Sedlmeir, H. G. L. Schwefel, and K. Buse, "Whispering gallery modes at the rim of an axisymmetric optical resonator: analytical versus numerical description and comparison with experiment," Opt. Express **21**, 30683–30692 (2013).
30. T. Carmon, H. G. L. Schwefel, L. Yang, M. Oxborrow, A. D. Stone, and K. J. Vahala, "Static envelope patterns in composite resonances

generated by level crossing in optical toroidal microcavities," Phys. Rev. Lett. **100**, 103905 (2008).
31. J. Wiersig, "Formation of long-lived, scarlike modes near avoided resonance crossings in optical microcavities," Phys. Rev. Lett. **97**, 253901 (2006).
32. U. Schlarb and K. Betzler, "Influence of the defect structure on the refractive indices of undoped and mg-doped lithium niobate," Phys. Rev. B **50**, 751–757 (1994).
33. S. Ramelow, A. Farsi, S. Clemmen, J. S. Levy, A. R. Johnson, Y. Okawachi, M. R. E. Lamont, M. Lipson, and A. L. Gaeta, "Strong polarization mode coupling in microresonators," Opt. Lett. **39**, 5134–5137 (2014).
34. W. Weng and A. N. Luiten, "Mode-interactions and polarization conversion in a crystalline microresonator," Opt. Lett. **40**, 5431–5434 (2015).
35. D. V. Strekalov, H. G. L. Schwefel, A. A. Savchenkov, A. B. Matsko, L. J. Wang, and N. Yu, "Microwave whispering-gallery resonator for efficient optical up-conversion," Phys. Rev. A. **80**, 033810 (2009).
36. M. Leidinger, S. Fieberg, N. Waasem, F. Kühnemann, K. Buse, and I. Breunig, "Comparative study on three highly sensitive absorption measurement techniques characterizing lithium niobate over its entire transparent spectral range," Opt. Express **23**, 21690–21705 (2015).
37. M. Goryachev, N. Kostylev, and M. E. Tobar, "Single-photon level study of microwave properties of lithium niobate at millikelvin temperatures," Phys. Rev. B **92**, 060406 (2015).
38. N. G. Pavlov, N. M. Kondratyev, and M. L. Gorodetsky, "Modeling the whispering gallery microresonator-based optical modulator," Appl. Opt. **54**, 10460–10466 (2015).
39. C. Javerzac-Galy, K. Plekhanov, N. Bernier, L. D. Toth, A. K. Feofanov, and T. J. Kippenberg, "On-chip microwave-to-optical quantum coherent converter based on a superconducting resonator coupled to an electro-optic microresonator," arXiv:1512.06442 (2015).
40. S. Huang, "Quantum state transfer in cavity electro-optic modulators," Phys. Rev. A **92**, 043845 (2015).
41. D. Bozyigit, C. Lang, L. Steffen, J. M. Fink, C. Eichler, M. Baur, R. Bianchetti, P. J. Leek, S. Filipp, M. P. da Silva, A. Blais, and A. Wallraff, "Antibunching of microwave-frequency photons observed in correlation measurements using linear detectors," Nat. Phys. **7**, 154–158 (2011).
42. R. W. Andrews, A. P. Reed, K. Cicak, J. D. Teufel, and K. W. Lehnert, "Quantum-enabled temporal and spectral mode conversion of microwave signals," Nat. Commun. **6**, 10021 (2015).
43. G. Schunk, U. Vogl, D. V. Strekalov, M. Förtsch, F. Sedlmeir, H. G. L. Schwefel, M. Göbelt, S. Christiansen, G. Leuchs, and C. Marquardt, "Interfacing transitions of different alkali atoms and telecom bands using one narrowband photon pair source," Optica **2**, 773–778 (2015).